On the opposing roles of the Boussinesq and non-Boussinesq baroclinic torques in surface gravity wave propagation

Eyal Heifetz[1], Ron Maor[1] and Anirban Guha[2,3*]

[1]*Department of Geophysics, Porter school of the Environment and Earth Sciences, Tel Aviv University, Tel Aviv 69978, Israel.*
[2]*School of Science and Engineering, University of Dundee, Nethergate, Dundee DD1 4HN, U.K.*
[3]*Institute of Coastal Research, Helmholtz-Zentrum Geesthacht, Geesthacht, 21502 Germany.*

[*]*Correspondence to: Email: anirbanguha.ubc@gmail.com*

Here we suggest an alternative understanding of the surface gravity wave propagation mechanism based on the baroclinic torque, which operates to translate the interfacial vorticity anomalies at the air-water interface. We demonstrate how the non-Boussinesq term of the baroclinic torque acts against the Boussinesq one to hinder wave propagation. By standard vorticity inversion and mirror imaging, we then show how the existence of the bottom boundary affects the two types of torque. Since the opposing non-Boussinesq torque results solely from the mirror image, it vanishes in the deep water limit and its magnitude is half of the Boussinesq torque in the shallow water limit. This reveals that Boussinesq approximation is valid in the deep water limit, even though the density contrast between air and water is large. The mechanistic roles, played by the Boussinesq and non-Boussinesq parts of the baroclinic torque, remain obscured in the standard derivation where the time-dependent Bernoulli equation is implemented instead of the interfacial vorticity equation. Finally, we note on passing that the Virial theorem for surface gravity waves can be obtained solely from considerations of the dynamics at the air-water interface.

1. Introduction

The fundamental theory of linear surface gravity waves was founded in the 18th and the early 19th centuries by pioneers like Laplace, Lagrange, Poisson, and Cauchy (Craik 2004). The standard derivation of the dispersion relation, based on the potential flow theory, is a well known procedure considered in almost all standard textbooks in fluid dynamics (e.g. see Kundu *et al.* (2016)).

Recently, there has been a growing body of literature (Holmboe 1962; Sakai 1989; Baines and Mitsudera 1994; Caulfield 1994; Harnik *et al.* 2008; Rabinovich *et al.* 2011; Carpenter *et al.* 2013; Guha and Lawrence 2014; Heifetz and Mak 2015) dealing with stratified shear flow instability that treats the dynamics of density discontinuity surfaces as *interfacial vorticity waves*[*]. This approach provides a mechanistic rationalization for Taylor-Caulfield and Holmboe instabilities, and also paves the path for efficient vortex-method-based computation schemes to simulate the nonlinear evolution, including wave-breaking (Bhardwaj and Guha 2018). However, while exploring these relatively complex problems, the analysis of surface gravity waves - probably the

simplest setup of a density discontinuity - in terms of interfacial vorticity waves has been "left behind". Hence, here we suggest an alternative derivation of surface gravity waves, based on the above-mentioned approach. To avoid confusion, we emphasize here that this work uses standard techniques of vorticity inversion and boundary mirror images in order to focus on the wave propagation mechanism rather than on the modelling of surface waves as vortex sheets, a well-known technique pioneered by Baker *et al.* (1982).

This article is organized as follows. In section 2, we derive and analyze the interfacial vorticity equations and then in section 3, we implement them to obtain the dispersion relation. Special care is given to the deep and the shallow-water limits. In section 4 we derive surface waves' energy from the interfacial fields. Finally, we close by discussing the results in section 5.

2. Interfacial vorticity dynamics

Assuming an incompressible, inviscid flow the governing continuity and momentum equations read

$$\nabla \cdot \mathbf{u} = 0, \quad \frac{D\rho}{Dt} = 0, \tag{2.1a,b}$$

$$\frac{D\mathbf{u}}{Dt} = -g\hat{\mathbf{k}} - \frac{1}{\rho}\nabla p, \tag{2.1c}$$

---

[*]We define any linear interfacial wave that propagates due to vorticity anomalies across the interface as a vorticity wave. Hence Rossby waves, gravity waves, capillary waves, Alfvén waves are all vorticity waves by this definition.

where $D/Dt \equiv \partial/\partial t + \mathbf{u} \cdot \nabla$ is the material derivative, $\mathbf{u}$, ρ, p, g and $\hat{\mathbf{k}}$ respectively denote velocity, density, pressure, gravity and the vertical unit vector. The vorticity equation is obtained by taking the curl of Equation 2.1c:

$$\frac{D\boldsymbol{\omega}}{Dt} = \underbrace{(\boldsymbol{\omega} \cdot \nabla)\mathbf{u}}_{\text{Stretching}} + \underbrace{\frac{1}{\rho^2}\nabla\rho \times \nabla p}_{\text{Baroclinic}}, \qquad (2.2)$$

where $\boldsymbol{\omega} \equiv \nabla \times \mathbf{u}$ is the vorticity. The first term on the RHS is the vortex stretching term that would be absent in 2D flows. The second term signifies the baroclinic torque when isopycnals and isobars are crossing. In general, this term can be divided into two parts – *Boussinesq* and *non-Boussinesq*.

Consider now the 2D (x, z) setup of hydrostatic background

$$\frac{d\overline{p}}{dz} = -\overline{\rho}g, \qquad (2.3)$$

where $\overline{p}$ and $\overline{\rho}$ respectively denote the mean pressure and density. Linearisation with respect to Equations 2.3, 2.1a,b and 2.1c yield

$$\frac{\partial u'}{\partial x} + \frac{\partial w'}{\partial z} = 0, \qquad (2.4a)$$

$$\frac{\partial \rho'}{\partial t} = -w'\frac{d\overline{\rho}}{dz}, \qquad (2.4b)$$

$$\frac{\partial u'}{\partial t} = -\frac{1}{\overline{\rho}}\frac{\partial p'}{\partial x}, \qquad (2.5a)$$

$$\frac{\partial w'}{\partial t} = -\frac{1}{\overline{\rho}}\frac{\partial p'}{\partial z} - \frac{\rho'}{\overline{\rho}}g, \qquad (2.5b)$$

where the primes denote perturbation quantities. *Hereafter, the primes will be dropped so that any variable without an overbar will denote a perturbation quantity.*

Defining the 2D vorticity[†] perturbation as

$$q = \frac{\partial w}{\partial x} - \frac{\partial u}{\partial z}, \qquad (2.6)$$

the 2D version of Equation 2.2 under hydrostatic balance yields

$$\frac{\partial q}{\partial t} = \underbrace{-\frac{g}{\overline{\rho}}\frac{\partial \rho}{\partial x}}_{T_1 \equiv \text{Boussinesq baroclinic}} + \underbrace{\left[-\frac{1}{\overline{\rho}^2}\left(\frac{d\overline{\rho}}{dz}\frac{\partial p}{\partial x}\right)\right]}_{T_2 \equiv \text{Non-Boussinesq baroclinic}}. \qquad (2.7)$$

The two terms in the RHS of Equation 2.7 emanate from the baroclinic term appearing in the RHS of Equation 2.2. Both T_1 and T_2 point in the negative y direction, in agreement with the definition of q. The vorticity can be generated from two baroclinic sources:

(i) $T_1 \equiv -(g/\overline{\rho})\partial\rho/\partial x$: denotes the "Boussinesq baroclinic torque". It results from the buoyancy restoring force acting to flatten a displaced density interface to its initial unperturbed horizontal position. Therefore, it generates the horizontal shear of the vertical velocity, $\partial w/\partial x$, in q; see Figure 1a.

(ii) $T_2 \equiv -(1/\overline{\rho}^2)(d\overline{\rho}/dz)(\partial p/\partial x)$: denotes the "non-Boussinesq baroclinic generation of vorticity", arises out of the density variations in the inertial terms, and is completely independent of the gravitational effects. This term vanishes if Boussinesq approximation (which, in a simplified sense, implies $\overline{\rho} \approx \text{const.}$ in Equation 2.7) is invoked. Alternatively, if we assumed Boussinesq approximation from the onset, then Equations 2.5a–2.5b would have resulted in Equation 2.7 with $T_2 \equiv 0$. T_2 results from the

---

[†]q points in the negative y direction in order to follow the convention in which counterclockwise (clockwise) rotation is associated with positive (negative) values of vorticity.
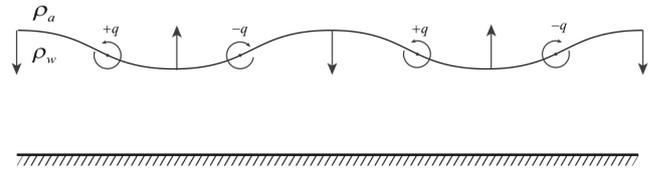
(a) The Boussinesq Mechanism
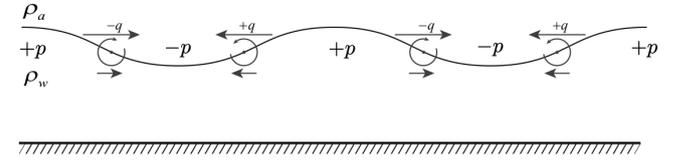
(b) The non-Boussinesq Mechanism

Figure 1. Schematic illustration of the air-water interface (wavy line); density of air and water are respectively ρ_a and ρ_w. (a) The vertical arrows denote vertical velocity generated by the Boussinesq term (T_1), contributing to the $\partial w/\partial x$ in q. (b) The non-Boussinesq term (T_2) is a scaled horizontal perturbation pressure gradient force generating vertical shear of the horizontal velocity, $-\partial u/\partial z$, and thus contributes to the generation of q. In both (a) and (b), the generated q is shown by circular arrows.

decrease with height of the mean density $\overline{\rho}$. Consequently, a horizontal perturbation pressure gradient accelerates the upper lighter material faster than the heavier material below it. This accounts to the vertical shear of the horizontal velocity, $-\partial u/\partial z$, in q; see Figure 1b (a more detailed analysis can be found in Heifetz and Mak (2015)).

Note that under situations when the displacement and the pressure perturbations correlate, T_1 and T_2 act against each other in generating vorticity. This will be shown to be the case for the air-water interface – for surface gravity waves over water of finite depth, a lift up of the interface is associated with a positive density anomaly and thus with a positive pressure perturbation.

The linearized kinematic condition at an interface (e.g. air-water free surface) is given by

$$\frac{\partial \eta}{\partial t} = w, \qquad (2.8)$$

where η denotes the free surface displacement. One can combine Equations 2.4b and 2.8 to obtain

$$\rho = -\eta\frac{d\overline{\rho}}{dz}. \qquad (2.9)$$

Equations 2.9 and 2.7 can be combined together, yielding

$$\frac{\partial q}{\partial t} = -N^2\frac{\partial}{\partial x}\left(\eta - \frac{p}{\overline{\rho}g}\right), \qquad (2.10)$$

where $N(z) \equiv \sqrt{-(g/\overline{\rho})d\overline{\rho}/dz}$ is the Brunt-Väisälä frequency. The RHS of Equation 2.10 indicates that close to hydrostaticity of the perturbations, T_1 and T_2 are of the same order of magnitude. Using Equation 2.5a we can rewrite Equation 2.10 as:

$$\frac{\partial}{\partial t}\left(q + \frac{N^2}{g}u\right) = -N^2\frac{\partial \eta}{\partial x}, \qquad (2.11)$$

where we note that the term T_2 is now the second term of the LHS.

2.1. Surface gravity waves

Consider now the standard setup of the air-water interface, at rest at $z = 0$. The water depth is H, while the air above is unbounded.

The mean density can be written as

$$\overline{\rho}(z) = \begin{cases} \rho_a \to 0, & 0 < z < \infty, \\ \rho_w, & -H < z < 0, \end{cases} \quad (2.12)$$

yielding $N^2 = 2g\delta(z)$, where δ denotes the Dirac delta function (if ρ_a is not neglected, g would be replaced by the reduced gravity). Equation 2.11 therefore implies that the vorticity perturbation will be generated only at the air-water interface, giving rise to an undulating vortex sheet. We wish to describe the gravity wave dynamics solely from the vorticity dynamics of this interface. For modal solution of the form

$$q = \hat{q}_0 \delta(z) e^{ik(x-ct)}, \quad (2.13)$$

where the subscript '0' indicates evaluation at $z = 0$, $\hat{q}_0$ denotes the vorticity amplitude and c is the phase speed. The vorticity can be inverted to obtain the streamfunction $\psi = \nabla^{-2}q$ to express the velocity field

$$(u, w) = \left(-\frac{\partial}{\partial z}, \frac{\partial}{\partial x}\right)\psi.$$

Using the Green function approach we can write:

$$\psi = \nabla^{-2}q = \int_{-H}^{\infty} q\, G(z, z', k) dz'$$

$$= \hat{q}_0 G(z, 0, k) e^{ik(x-ct)} = \hat{\psi}(z) e^{ik(x-ct)}, \quad (2.14)$$

where the Green function G satisfies Helmholtz-Poisson's equation:

$$\left(-k^2 + \frac{\partial^2}{\partial z^2}\right) G(z, 0, k) = \delta(z). \quad (2.15)$$

The structure of the Green function results from the assumption of potential flow dynamics above and below the air-water discontinuity, where the jump in u across the interface yields the vorticity delta function of Equation 2.13. Furthermore, we apply the evanescent condition $w(z \to \infty) \to 0$, and the solid impenetrable boundary condition, $w(z = -H) = 0$, implying $G(z = \infty, 0, k) = G(z = -H, 0, k) = 0$.

The dynamics finally boils down to finding the modal solution that simultaneously satisfies Equation 2.8 and Equation 2.11 at the interface. Writing $\eta = \hat{\eta}_0 e^{ik(x-ct)}$ and recall that $N^2 = 2g\delta(z)$, we obtain

$$c = \frac{i}{k}\frac{\hat{w}_0}{\hat{\eta}_0}, \quad (2.16a)$$

$$c = \frac{2g\hat{\eta}_0}{\hat{q}_0 + 2\hat{u}_0}, \quad (2.16b)$$

where both $(\hat{u}_0, \hat{w}_0)$ are expressed in terms of $\hat{q}_0$. Equation 2.16a, which results from the kinematic condition 2.8, reveals that for waves propagating in the positive (negative) x direction, the vertical velocity is located a quarter of wavelength to the right (left) of the displacement anomaly (see Figure 2). Equation 2.16b, which results from the interfacial vorticity equation 2.11, indicates that $(q_0 + 2u_0)$ and η_0 should be in phase (anti-phase) for positive (negative) wave propagation. While the former is a general property of any transverse wave, the latter will be clarified in the next section. Equation 2.16b can be obtained as well from the conventional dynamic condition. Writing the time dependent Bernoulli equation for the potential flow just below the interface:

$$-\frac{\partial\phi}{\partial t} = \frac{\mathbf{u}^2}{2} + \frac{p}{\rho} + gz, \quad (2.17)$$

where the velocity potential ϕ satisfies $\mathbf{u} = \nabla\phi$, we obtain after linearisation that just below the wavy interface $\partial\phi/\partial t = -g\eta$,

(a)

(b)
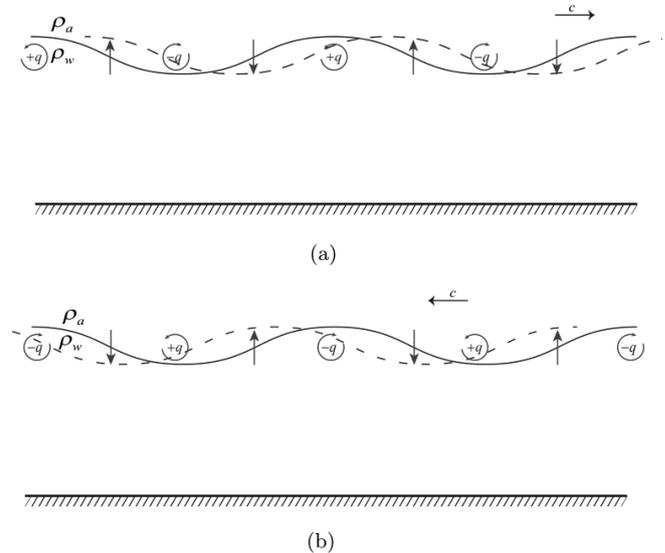
Figure 2. Schematic illustration of the propagation of surface gravity waves. (a) When the interface vorticity (indicated by circular arrows) and displacement (indicated by the solid undulating line) are in phase, the vertical velocity (indicated by the vertical arrows) induced by the perturbation vorticity is located a quarter of wavelength to the right of the displacement, thus translating the displacement (the dashed undulating line) in the positive x direction (Equation 2.16a). (b) Same as in (a), except that now the wave propagates in the negative x direction as the vorticity and the displacement anomalies are in anti-phase.

so that $c = g\hat{\eta}_0/ik\hat{\phi}_0$, where $ik\hat{\phi}_0 = \hat{q}_0/2 + \hat{u}_0$. The first term in the RHS is the Boussinesq contribution to the velocity potential, whereas the second is the non-Boussinesq one. Nonetheless, the dynamic condition by itself does not allow us to straightforwardly separate the Boussinesq and the Non-Boussinesq dynamics.

We also note in passing an important aspect of transverse waves by simply analyzing Equation 2.16a. The maximum (or minimum) phase speed occurs when $\partial c/\partial k = 0$, which gives for a reference wave amplitude displacement $\hat{\eta}_0$:

$$\frac{\partial\hat{w}_0}{\partial k} = \frac{\hat{w}_0}{k} \implies \hat{w}_0 = \alpha k, \quad (2.18)$$

where α is a constant. Substituting this relation in Equation 2.16a yields

$$c_{max} = \left|\frac{\alpha}{\hat{\eta}_0}\right|. \quad (2.19)$$

The above equation shows that the maximum phase speed is *independent* of the wavenumber k, implying that in the fast phase speed limit, transverse waves are non-dispersive. It is important to note that the above relation is *independent* of the dynamic condition and hence applicable to any transverse wave. This simple derivation provides a mathematical justification of the well-known fact that in the shallow water limit, the phase speed is maximum and the waves are non-dispersive.

3. Dispersion relation analysis

3.1. *deep-water limit*

Consider first the deep-water (hereafter DW) limit, that is, $kH \to \infty$. In this case, the Green function $G_{DW} = -e^{-k|z|}/2k$, which yields

$$\psi = -\frac{\hat{q}_0}{2k}e^{-k|z|}e^{ik(x-ct)}. \quad (3.1)$$

In Figure 3 the velocity field associated with ψ is plotted. The evanescent structure of the vector field away from the interface shows that both the divergence and the vorticity fields are zero everywhere ($\partial u/\partial x = -\partial w/\partial z$ and $\partial w/\partial x = \partial u/\partial z$) except at the interface, where the vorticity goes to infinity in
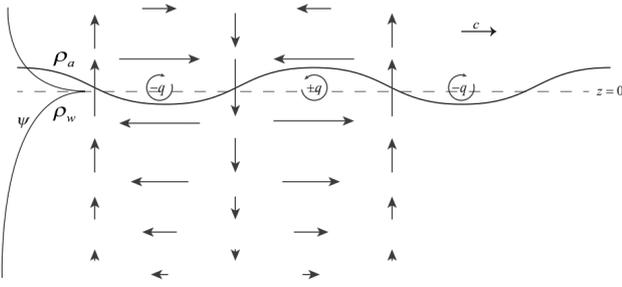
Figure 3. The velocity field of the rightward propagating surface gravity wave in the deep-water limit. The vertical structure of the deep-water streamfunction (Equation 3.1) is illustrated in the left. Due to its evanescent structure away from the interface, the flow is everywhere non-divergent. It is also irrotational everywhere except at the interface, where the jump in the horizontal velocity across the interface generates a delta function in vorticity. For leftward propagating waves in the deep water limit, the velocity field is the same but the displacement is in anti-phase with the vorticity anomaly.

magnitude since the jump in the sign of u across the interface generates the vortex sheet. Since $u(0^-) = -u(0^+)$, we have $u_0 = 0$. This implies that the non-Boussinesq baroclinic torque term in Equation 2.11 vanishes in the DW limit. Furthermore, from Equation 3.1 we obtain, $\hat{w}_0 = -i\hat{q}_0/2$, thus Equations 2.16a–2.16b gives the familiar DW phase speed relation:

$$c = \frac{\hat{q}_0}{2k\hat{\eta}_0} = \frac{2g\hat{\eta}_0}{\hat{q}_0} = \pm\sqrt{\frac{g}{k}}, \qquad (3.2)$$

corresponding to:

$$\left(\frac{\hat{q}_0}{\hat{\eta}_0}\right)^{\pm} = \pm 2\sqrt{gk}. \qquad (3.3)$$

Hence, when the interface displacement and vorticity are in (anti) phase the wave propagates to the (left) right (see Figure 3). Such behavior is common with other types of interfacial vorticity waves such as capillary (Biancofiore *et al.* 2017), Rossby (Hoskins *et al.* 1985) and Alfven (Heifetz *et al.* 2015) waves.

We note here that although we are considering a "non-Boussinesq" density jump (air-water interface), the non-Boussinesq effect is *completely absent* for the deep-water limit. In other words, this implies that the Boussinesq effects are not confined to "small density variations", as is conventionally understood. A similar conclusion has been obtained by Guha and Raj (2018) using detailed scaling arguments.

3.2. Finite depth

In the finite depth case, the effect of the impenetrability of the solid boundary, located at a finite distance ($z = -H$), can be represented equivalently by replacing that boundary by an anti-phased undulating vortex sheet (mirror image of the one at $z = 0$), located at $z = -2H$. This yields

$$\psi = -\frac{\hat{q}_0}{2k}\left(e^{-k|z|} - e^{-k|z+2H|}\right)e^{ik(x-ct)}, \qquad (3.4)$$

which indeed vanishes at $z = -H$, satisfying impenetrability. Furthermore, this anti-phased mirror vortex sheet reduces the vertical velocity at the interface at $z = 0$ as it induces an evanescent vertical velocity of opposite sign (see Figure 4):

$$\hat{w}_0 = -i\frac{\hat{q}_0}{2}\left(1 - e^{-2kH}\right). \qquad (3.5)$$

We readily observe that when $kH \to \infty$, we recover $\hat{w}_0 = -i\hat{q}_0/2$, i.e., the vertical velocity in the deep-water limit. Due to
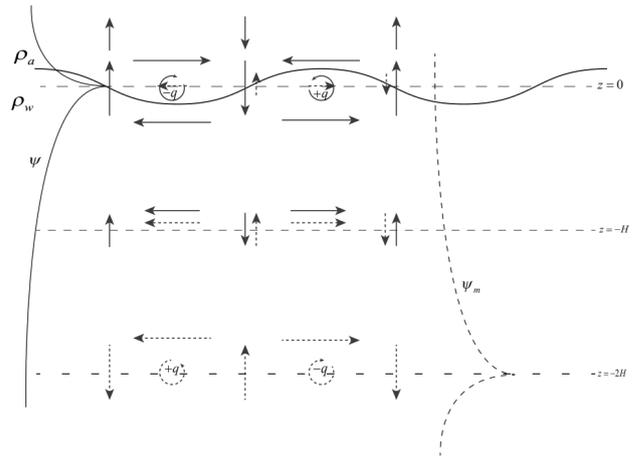
Figure 4. Same as in Figure 3 but for the finite depth case. Here, the velocity field results from Equation 3.4, which is the superposition of the deep-water streamfunction (indicated in Figure 3 by the solid evanescent profile on the left) and its anti-phase mirror image streamfunction ψ_m, whose evanescent structure away from $z = -2H$ is shown on the right with dashed line. The superposition of the induced vertical velocity from the air-water interface and its mirror image completely cancel each other at $z = -H$, thereby satisfying impenetrability. Moreover, the vertical velocity induced by the mirror image on the interface at $z = 0$ is in anti-phase with the local self-induced vertical velocity. Therefore, according to Equation 2.16a and the illustration in Figure 2, this slows the interface propagation. Furthermore, the horizontal velocity at the interface is non-zero (unlike the deep-water case) since it has a contribution from the mirror image, which is in phase with the vorticity anomaly at the interface. This stands in agreement with Equation 2.16b as it decreases the phase speed magnitude. The latter effect is due to the non-Boussinesq baroclinic torque (c.f. Equations 2.10–2.11 and Figure 1b).

the presence of a solid boundary at a finite depth, the phase speed should decrease according to Equation 2.16a. This reduction in the phase speed magnitude is obtained from Equation 2.16b as well. Indeed, as illustrated in Figure 4, the anti-phased mirror image vortex sheet at $z = -2H$ induces a horizontal velocity u which is in phase with the vortex sheet at $z = 0$. In fact, the sole contribution to u_0 is from the anti-phased mirror image vortex sheet. From Equation 3.4, $\hat{u}_0$ is found to be

$$\hat{u}_0 = -\left(\frac{\partial\psi}{\partial z}\right)_{z=0} = \frac{\hat{q}_0}{2}e^{-2kH}. \qquad (3.6)$$

Substituting Equation 3.6 back in Equation 2.11 we obtain

$$\frac{\partial q}{\partial t} = -\frac{N^2}{(1 + e^{-2kH})}\frac{\partial\eta}{\partial x}. \qquad (3.7)$$

Hence the interface displacement slope, $-\partial\eta/\partial x$, is able to produce less vorticity ($\partial q/\partial t$); the non-Boussinesq term e^{-2kH} appearing in the denominator of the RHS is always greater than 1. Stated differently, the two terms in the RHS of Equation 2.10 work against each other (while the first Boussinesq term T_1 dominates the second non-Boussinesq term T_2), since now the interface displacement correlates with the pressure perturbation there (c.f. Figure 1 and Figure 4). Substituting $(\hat{u}_0, \hat{w}_0)$ in Equations 2.16a–2.16b gives

$$c = \frac{\hat{q}_0}{2k\hat{\eta}_0}\left(1 - e^{-2kH}\right) = \frac{2g\hat{\eta}_0}{\hat{q}_0\left(1 + e^{-2kH}\right)} = \pm\sqrt{\frac{g}{k}\tanh(kH)}, \qquad (3.8)$$

corresponding to:

$$\left(\frac{\hat{q}_0}{\hat{\eta}_0}\right)^{\pm} = \pm 2\sqrt{\frac{gk}{1 - e^{-4kH}}}. \qquad (3.9)$$

Equation 3.8 is the familiar dispersion relation of intermediate depth surface gravity waves.
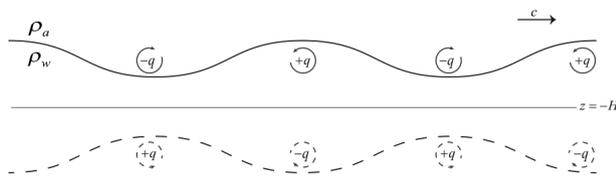
Figure 5. The wave structure for the shallow-water limit can be viewed as a series of dipole-like bulges due to the vorticity interface and its anti-phased mirror image. In this illustration the interface anomaly is highly exaggerated in order to show the effect. When the wave propagates to the right (as shown here), the positive vorticity anomaly is above the negative one within the bulges. For leftward propagation (not shown here) the structure is upside down.

3.3. Shallow-water limit

The shallow-water (hereafter SW) limit of $kH \ll 1$ is also interesting to analyze from this perspective. The vertical structure of the streamfunction becomes independent of the wavenumber when the vortex sheet and its anti-phased mirror image become very close to each other, thereby generating a series of dipole-like structures (Figure 5). This reflects in the phase speed, which now becomes independent of the wavenumber. As can be seen from Equation 3.4, under the shallow-water limit

$$\psi = \frac{\hat{q}_0}{2} \left(|z| - |z + 2H| \right) e^{ik(x-ct)} , \qquad (3.10)$$

yielding $(\hat{u}_0, \hat{w}_0) = (\frac{1}{2}, -ikH)\hat{q}_0$. Substitution of this in Equations 2.16a–2.16b gives

$$c = H\frac{\hat{q}_0}{\hat{\eta}_0} = g\frac{\hat{\eta}_0}{\hat{q}_0} = \pm\sqrt{gH} , \qquad (3.11)$$

corresponding to:

$$\left(\frac{\hat{q}_0}{\hat{\eta}_0} \right)^{\pm} = \pm\sqrt{\frac{g}{H}} . \qquad (3.12)$$

Again, one can easily recognize that Equation 3.11 is the familiar dispersion relation for shallow-water waves. It is straightforward to verify that in the SW limit the magnitude of the opposing non-Boussinesq torque is equal to half of the Boussinesq one.

4. Gravity wave energy from the interfacial fields

Defining $K \equiv \overline{\rho} \left(u^2 + w^2 \right) /2$ as the kinetic and $P \equiv \overline{\rho}(N\eta)^2/2$ as the potential energies, it is straightforward to deduce from Equations 2.4a–2.5b that

$$\frac{\partial}{\partial t} \langle K \rangle = -\langle w\rho g \rangle = -\frac{\partial}{\partial t} \langle P \rangle , \qquad (4.1)$$

where the domain integration operator is defined as

$$\langle \ldots \rangle \equiv \frac{1}{\lambda} \int_{x}^{x+\lambda} \int_{z=-H}^{\infty} (\ldots) dz dx , \qquad (4.2)$$

where $\lambda = 2\pi/k$ is the wavelength. Equation 4.1 indicates that the total wave energy $\langle E \rangle = \langle K + P \rangle$ is conserved. After integration by parts it can be shown that

$$\langle K \rangle = -\frac{1}{2} \left\langle \psi \left(\overline{\rho}q - \frac{d\overline{\rho}}{dz}u \right) \right\rangle . \qquad (4.3)$$

Substituting Equations 2.13, 3.4 and 3.6 we obtain

$$\langle K \rangle = \frac{\rho_w}{16k} \left(1 - e^{-4kH} \right) \hat{q}_0^2 , \qquad (4.4)$$

and using Equation 3.9 we obtain the familiar result

$$\langle K \rangle = \frac{1}{4} \rho_w g \hat{\eta}_0^2 . \qquad (4.5)$$

Finally, substituting $N^2 = 2g\delta(z)$ in $P \equiv \overline{\rho}(N\eta)^2/2$ we recover the well known equi-partition energy relation: $\langle K \rangle = \langle P \rangle$, as demanded by the Virial theorem (Bühler 2014).

5. Discussion

In geophysical fluid dynamics, gravity waves are often associated with the fast divergent component of the flow, whereas the vortical component is associated with the slower quasi-balanced Rossby wave-like dynamics. For the latter, the vertical component of vorticity (or potential vorticity) equation plays the key role in understanding its evolution and vorticity inversion is used to obtain the far field velocity field induced by the vorticity field. The fact that interfacial gravity waves, generated by density discontinuities, can be treated as undulated vortex sheets has been acknowledged a while ago (e.g. Baker *et al.* (1982)), however to the best of our knowledge, its spanwise (i.e. the meridional direction for zonal wave propagation) vorticity equation has not been implemented to understand the propagation mechanism of gravity waves.

Analysis of the spanwise vorticity equation reveals that the interfacial vorticity is translated by the baroclinic torque acting on the interface when the dynamics deviates from the rest state of hydrostatic balance. The baroclinic torque has two components - Boussinesq and non-Boussinesq, which tend to act against each other, where the Boussinesq always overwhelms the non-Boussinesq. The non-Boussinesq component depends on the perturbation horizontal pressure gradient force across the interface, which in turn accelerates the zonal perturbation velocity there. Using vorticity inversion and mirror imaging technique for the bottom boundary, we see that the zonal velocity at the interface results solely from the vorticity induced by the mirror imaging. Therefore, in the deep water limit, this contribution vanishes. Hence, the non-Boussinesq dynamics vanishes despite of the large density contrast at the water-air interface. When the water depth decreases, the magnitude ratio of the non-Boussinesq and Boussinesq baroclinic torques increases, reaching the value of $1/2$ in the shallow water limit. The same dispersion relation is obviously obtained if the conventional dynamic condition of the time-dependent Bernoulli equation is use instead, however it is not clear from the latter how to disentangle the non-Boussinesq dynamics from the Boussinesq one.

Even for infinite depth, the non-Boussinesq torque should still be taken into account when multiple density interfaces exist (Heifetz and Mak 2015; Guha and Raj 2018). This is because the vortex sheet gravity waves induce far field horizontal fields on each other and thereby activate the non-Boussinesq dynamics. As opposed to the mirror images, which are always in anti-phase with the vortex sheet interface, the gravity waves moves relative to each other when background shear is present. Thus a non-Boussinesq stratified shear flow action at a distance between counter-propagating interfacial gravity waves can lead to a phase locking resonant instability in a similar (though more complex) manner of the barotropic and baroclinic instability between Rossby waves, described in Hoskins *et al.* (1985).

The undulating vortex sheet understanding of surface gravity waves shares some similarities with the Bretherton delta function potential vorticity representation of the solid boundary condition in baroclinic quasi-geostrophic setups (Bretherton 1966). Specifically, here we showed that the total, domain integrated energy of the gravity waves can be obtained solely from evaluating the dynamical fields at the air-water interface, similar to the evaluation of the total energy of the discrete spectrum in the Eady model solely from the boundary fields (Eady 1949; Heifetz *et al.* 2004).

Prepared using qjrms4.cls

References

Baines PG, Mitsudera H. 1994. On the mechanism of shear flow instabilities. *J. Fluid Mech.* **276**: 327–342.

Baker GR, Meiron DI, Orszag SA. 1982. Generalized vortex methods for free-surface flow problems. *J. Fluid Mech.* **123**: 477–501.

Bhardwaj D, Guha A. 2018. Nonlinear modeling of stratified shear instabilities, wave breaking, and wave-topography interactions using vortex method. *Phys. Fluids* **30**(1): 014 102.

Biancofiore L, Heifetz E, Hoepffner J, Gallaire F. 2017. Understanding the destabilizing role for surface tension in planar shear flows in terms of wave interaction. *Phys. Rev. Fluids* **2**(10): 103 901.

Bretherton FP. 1966. Baroclinic instability and the short wavelength cut-off in terms of potential vorticity. *Q. J. Roy. Meteor. Soc.* **92**(393): 335–345.

Bühler O. 2014. *Waves and mean flows*. Cambridge University Press.

Carpenter JR, Tedford EW, Heifetz E, Lawrence GA. 2013. Instability in stratified shear flow: Review of a physical interpretation based on interacting waves. *Appl. Mech. Rev.* **64**(6): 060 801–17.

Caulfield CCP. 1994. Multiple linear instability of layered stratified shear flow. *J. Fluid Mech.* **258**: 255–285.

Craik AD. 2004. The origins of water wave theory. *Annu. Rev. Fluid Mech.* **36**: 1–28.

Eady ET. 1949. Long waves and cyclone waves. *Tellus* **1**(3): 33–52.

Guha A, Lawrence GA. 2014. A wave interaction approach to studying non-modal homogeneous and stratified shear instabilities. *J. Fluid Mech.* **755**: 336–364.

Guha A, Raj R. 2018. On the inertial effects of density variation in stratified shear flows. *Phys. Fluids* **30**(12): 126 603.

Harnik N, Heifetz E, Umurhan OM, Lott F. 2008. A buoyancy-vorticity wave interaction approach to stratified shear flow. *J. Atmos. Sci.* **65**(8): 2615–2630.

Heifetz E, Bishop CH, Hoskins BJ, Methven J. 2004. The counter-propagating rossby-wave perspective on baroclinic instability. i: Mathematical basis. *Q. J. Royal Meteorol. Soc.* **130**(596): 211–231.

Heifetz E, Mak J. 2015. Stratified shear flow instabilities in the non-Boussinesq regime. *Phys. Fluids* **27**(8): 086 601.

Heifetz E, Mak J, Nycander J, Umurhan OM. 2015. Interacting vorticity waves as an instability mechanism for magnetohydrodynamic shear instabilities. *J. Fluid Mech.* **767**: 199–225.

Holmboe J. 1962. On the behavior of symmetric waves in stratified shear layers. *Geophys. Publ* **24**: 67–113.

Hoskins BJ, McIntyre ME, Robertson AW. 1985. On the use and significance of isentropic potential vorticity maps. *Q. J. Roy. Meteor. Soc.* **111**(470): 877–946.

Kundu PK, Cohen IM, Dowling DR. 2016. Fluid mechanics.

Rabinovich A, Umurhan OM, Harnik N, Lott F, Heifetz E. 2011. Vorticity inversion and action-at-a-distance instability in stably stratified shear flow. *J. Fluid Mech.* **670**: 301–325.

Sakai S. 1989. Rossby-Kelvin instability: a new type of ageostrophic instability caused by a resonance between Rossby waves and gravity waves. *J. Fluid Mech.* **202**: 149–176.